JCB
Online Supplemental Material

Muro et al. http://www.jcb.org/cgi/doi/10.1083/jcb.200212079

Supplemental results and discussion

Rationale for the optimization of the splice sites

We demonstrated previously that the mEDA3′SS(A) + 5′SScons plasmid, which contains a hybrid FN–α-globin minigene with optimized 5′ and 3′ EDA splicing sites, generates mRNA with constitutively included-in EDA exon (Muro et al., 1998). In this plasmid, the natural 5′ splice site (CAG:GTA**TA**T) was mutated toward the 5′ splice site consensus sequence (CAG:GTA**AG**T) to improve its base complementarity to U1 RNA (Fig. S1 C). In the same way, the 3′ splicing site was replaced by that of the constitutively spliced-in second exon of the ApoA1 gene, resembling the 3′ splice site consensus sequence. To obtain constitutive exclusion of the FN-EDA exon from the mRNA, we constructed the mEDAΔEDA plasmid that had a deletion of 715 bp comprising the entire EDA exon (270 bp) and a small region of the flanking introns.

As there is tissue-specific regulation of the FN-EDA splicing pattern in vivo (Hynes, 1990; ffrench-Constant, 1995; Kornblihtt et al., 1996), both constructs were tested for efficiency of splicing by transient transfection in cell lines derived from different mouse organs having different EDA inclusion rate (unpublished data). Constitutive inclusion of the EDA exon was obtained with the mEDA3′SS(A) + 5′SScons plasmid in all cell types tested. As expected, the mEDAΔEDA plasmid produced only the EDA minus form in all cell types tested indicating that deletion of the EDA exon from the pre-mRNA did not alter the mRNA processing.

These results confirmed that both the optimization of the splicing sites of the EDA exon and its deletion lead to constitutive splicing independently of the cell type tested and opened the possibility of in vivo altering the alternative splicing pattern of the FN gene, and probably of other genes.

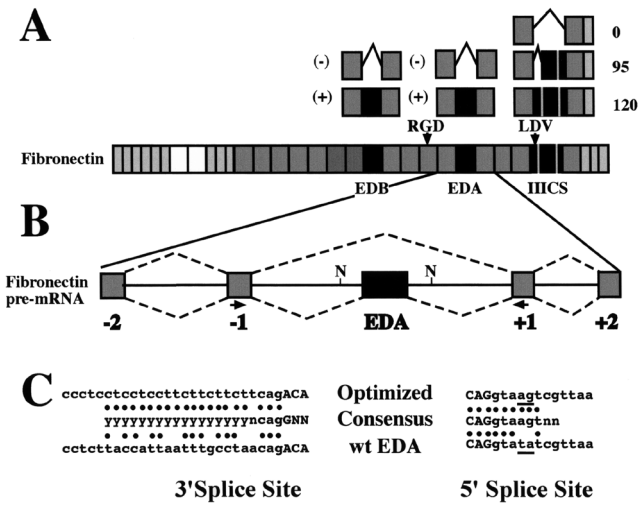

Figure S1. **The weak splicing junctions of the EDA exon are responsible for regulated splicing.** (A) Scheme of FN. The figure represents the longest FN polypeptide showing internal homologies. Constitutive (RGD) and alternatively spliced (LDV) cell-binding sites are indicated. Light gray, white, and gray squares represent Type I (40 aa), Type II (60 aa), and Type III (90 aa) homologies, respectively. Black squares represent the alternatively spliced exons. The possible splicing variants in mice are shown. (B) Schematic representation of the EDA gene region. The alternatively spliced forms are represented. Numbers indicate exons relative to the EDA exon. Each Type III homology is coded by two exons except for the EDA, EDB, and the ninth Type III homology. Arrows indicate primers used to analyze the EDA splicing by RT-PCR. "N" indicates the NdeI sites used for cloning purposes and for inserting "loxP" sites. FN exons and introns are shown as boxes and lines, respectively. (C) Comparison between the wild-type, mutated EDA splicing junctions, and the consensus ones. Dots indicate base identity. At the 5′ splice junctions, the two bases that were mutated are underlined.

RNase protection analysis

We tested, by RNase protection analysis, the effectiveness of the EDA splicing site modifications in adult liver of the FN transcripts in all the genotypes ($EDA^{wt/wt}$, $EDA^{+/+}$, $EDA^{-/-}$, $EDA^{+/-}$, $EDA^{-/wt}$, and $EDA^{+/wt}$).

The RNase protection method is extremely sensitive and used to determine, in a quantitative manner, specific RNAs of the tissue under analysis without any further amplification (Sambrook et al., 1989). A 420-bp sequence-specific hybridization ^{32}P-radiolabeled probe was prepared and hybridized to different liver total RNA samples from 2-mo-old mice of all different genotypes (Fig. S2 A). The FN RNA from the $EDA^{wt/wt}$ mice (Fig. S2, B and C, lanes 1 and 2) showed 98–99% of the 187 bases protected fragment, indicating almost complete EDA exon exclusion, in complete agreement with previous studies (Tamkun and Hynes, 1983; Kornblihtt et al., 1984). The FN mRNA prepared from $EDA^{+/+}$ mice showed only the 350-bases protected fragment, indicating constitutive inclusion of the EDA exon (Fig. S2, B and C, lanes 3 and 4) and the absence of alternative splicing of the EDA exon. The FN mRNA from $EDA^{-/-}$ mice showed the complete exclusion of the EDA exon (Fig. S2, B and C, lanes 5 and 6), as expected because the EDA exon was deleted from the genome. Heterozygous mice bearing one EDA^{+} allele showed values of EDA exon inclusion close to the expected 50% (Fig. S2, B and C, lanes 7, 8, 11, and 12). Analysis in the brain and spleen produced similar

results to those observed in the liver (unpublished data), except for the tissue-specific variation in the basal ratio of EDA inclusion of the EDA^{wt} allele.

Analysis of allele frequencies, offspring, and embryos

Mendelian frequency. Heterozygous crosses ($EDA^{+/wt} \times EDA^{+/wt}$ and $EDA^{-/wt} \times EDA^{-/wt}$) produced progeny within the expected Mendelian frequency, indicating that there was no intrauterine mortality. We observed 24.9% $EDA^{wt/wt}$, 52.2% $EDA^{+/wt}$, and 22.8% $EDA^{+/+}$ from 473 offspring born from heterozygous $EDA^{+/wt}$ mating pairs; and 27.1% $EDA^{wt/wt}$, 49.4% $EDA^{-/wt}$, and 23.5% $EDA^{-/-}$ from 332 offspring born from heterozygous $EDA^{-/wt}$ mating pairs (not significantly different from the expected Mendelian frequency by the χ^2 test; $c^2 = 1.355$ and $c^2 = 0.916$, for $EDA^{+/wt}$ and $EDA^{-/wt}$ matings, respectively).

Litter size and survival rate until weaning. The average litter size (mean ± SD) was 8.2 ± 2.3 and 7.5 ± 2.2 for each mating group ($EDA^{+/wt} \times EDA^{+/wt}$ and $EDA^{-/wt} \times EDA^{-/wt}$), respectively. Survival rate after birth, measured until weaning of the litter, was also indistinguishable between the $EDA^{+/+}$ and $EDA^{-/-}$ mice when compared with that of the $EDA^{wt/wt}$ littermates. The average litter size in crosses between homozygous mice of each genotype ($EDA^{-/-} \times EDA^{-/-}$ and $EDA^{+/+} \times EDA^{+/+}$) was normal, which did not differ significantly from that observed among the $EDA^{wt/wt}$ littermates and was within the range observed previously for heterozygous matings. The $EDA^{+/+}$ and $EDA^{-/-}$ matings produced on average six to seven litters, each spaced by 21–22 d, which is consistent with the normal mouse estrous cycle.

Somite number. Embryos (9.5 d p.c.) derived from timed matings of $EDA^{wt/wt}$, $EDA^{+/+}$, and $EDA^{-/-}$ mice were analyzed for the number of somites and shape. No differences were observed neither in the shape of the embryos nor in the number of somites (number of somites, mean ± SD: $EDA^{+/+}$: 22.7 ± 2.1, $n = 10$; $EDA^{-/-}$: 21.9 ± 2.5, $n = 25$; and $EDA^{wt/wt}$: 23.7 ± 2.6, $n = 30$).

Gain weight. Weight gain of 3-mo-old $EDA^{+/+}$ (mean ± SD, 34.3 ± 4.7, $n = 19$) and $EDA^{-/-}$ mice (35.0 ± 4.2, $n = 25$) did not differ significantly from that of $EDA^{wt/wt}$ mice weight (33.8 ± 3.4, $n = 18$).

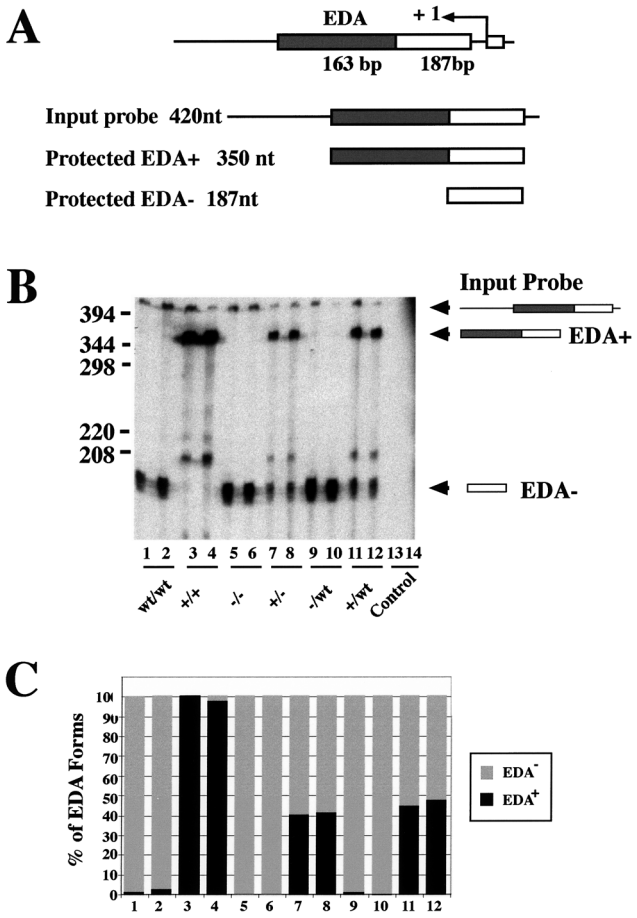

Figure S2. **Absence of alternative splicing in both EDA^+ and EDA^- FN alleles.** (A) Scheme of the RNase protection assay. The input probe and EDA^+-and EDA^--protected fragments are shown. FN sequences are indicated as boxes and plasmidic sequences as lines. (B) RNase protection assay of liver. 50 μg of liver RNA samples from 2-mo-old mice of all genotypes were hybridized with the antisense FN-EDA 420 bases radiolabeled probe. The digestion reaction generated protected EDA^+ (350 bases) and EDA^- (187 bases) fragments (indicated) and specific bands were quantitated by using a PhosphorImager and corrected by U content. (C) Graphical representation of the results shown in B. Black and gray rectangles represent the percentage of EDA^+ and EDA^- forms in each sample, respectively.

Northern blot analysis

To determine whether the observed decrease in FN protein levels in the $EDA^{+/+}$ mice was correlated to a decrease in the mRNA levels, we performed Northern blot analysis with total RNA isolated from the tissues having the higher decrease in FN levels (brain and heart) from 3-mo-old male mice. The 8.0-kb FN messenger was detected by a 711-bp cDNA probe, and the results from the $EDA^{wt/wt}$, $EDA^{+/+}$, and $EDA^{-/-}$ mice are shown in Fig. S3 A. No significant variations were observed in RNA samples from the brain and heart of $EDA^{+/+}$ mice. To correct for differences in RNA loading, the FN levels were normalized by two housekeeping genes (GAPDH and β-actin) showing similar results (Fig. S3, B–D).

TUNEL and caspase-3 analysis of skin wounds

Cell death and apoptosis-specific analysis were performed by the TUNEL and caspase-3 of the 7-d postwounding sections analyzed in Fig. 6 (8 and 16 wounds per genotype for TUNEL and caspase-3 experiments, respectively). We observed no significant differences in the number of positive cells between the different genotypes (Fig. S4).

Supplemental material and methods

Genotyping of progeny by Southern blot and PCR

For PCR analysis, 250–500 ng of genomic DNA was used for 30 cycles of PCR with the FN Nde Fwd and FN Nde Rev primers (5′-CTTCAGGGTGTCTACATAC-3′ and 5′-ACCGAGGTGTCTCACTTAG-3′, respectively). PCR products were separated in a 1% agarose gel and visualized by ethidium bromide staining (Fig. 2 C).

RNase protection assay

RNase protection analysis was performed as described previously (Ausubel et al., 1998). In brief, the sequence-specific hybridization probe (EDA) was cloned in pBSKSII and the antisense radiolabeled RNA was transcribed and gel purified. The RNA samples were hybridized overnight at 45°C with the radioactive labeled antisense transcript, and hybrids were digested with RNases A and T1. Protected fragments were separated on a sequencing 5% acrylamide/urea gels and analyzed by autoradiography. 20 μg of transfer RNA was used as a negative control. All experiments were repeated twice and in duplicates.

Synchronized matings and embryo analysis

Matings were done between homozygous mice of each genotype. One male was left with two females for half an hour in each case for each genotype and sexual intercourse was scored by the presence of a vaginal plug. Gross evaluation of the embryos was done exactly at day 9.5 after copulation. The embryos were carefully dissected under a stereomicroscope, fixed, and the number of somites was counted. Embryos were photographed at the same magnification.

Genotyping of progeny by Southern blot and PCR

Genomic DNA was prepared from tail samples as described previously (Laird et al., 1991). For Southern blot analysis, tail DNA was digested with HindIII and separated electrophoretically on an 0.8% agarose gel, blotted onto a nylon membrane (Z-Probe), and hybridized with a 300-bp radiolabeled DNA fragment containing the EDA + 1 exon (Fig. 2 B).

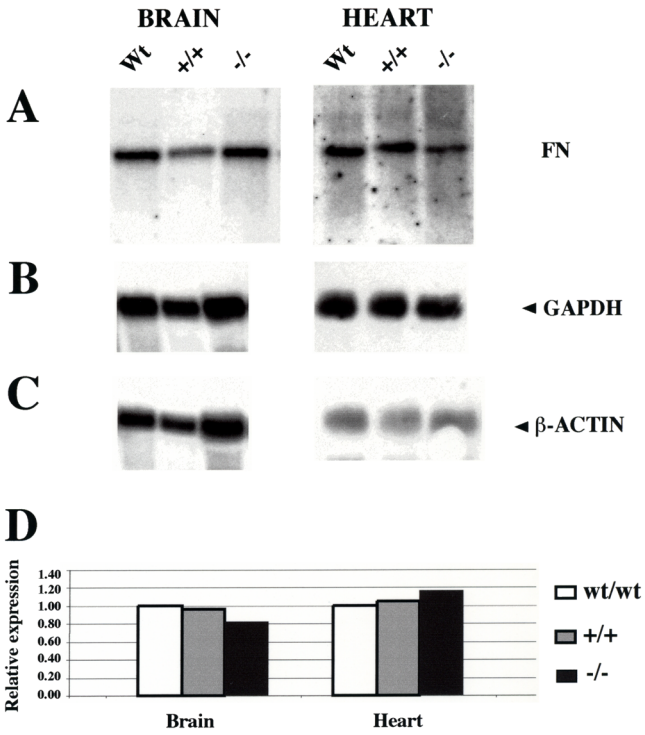

Figure S3. **Northern blot analysis of the FN mRNA expression.** Northern blot analysis of total RNA samples from brain and heart from adult mice (3-mo old; $EDA^{wt/wt}$, $EDA^{+/+}$, and $EDA^{-/-}$ mice). The same membrane used with the mFN probe was stripped after probing and used again with GAPDH and β-actin probes. (A) A 711-bp probe detected 7.8-kb FN mRNA in the different tissues. In the $EDA^{+/+}$ mouse, FN mRNA is slightly higher in all tissues due to the constitutive presence of the EDA exon in FN mRNA. (B and C) To correct for differences in RNA loading, the FN levels were normalized by two housekeeping genes (GAPDH and β-actin) showing similar results. A 300-bp and a 550-bp mouse cDNA probes were used to detect the GAPDH and the β-actin mRNAs, respectively, in the different tissues. (D) Graphical representation showing the relative levels of the FN mRNA in $EDA^{+/+}$ and $EDA^{-/-}$ mice with respect to the $EDA^{wt/wt}$ samples after normalization with GAPDH levels. A PhosphorImager was used for quantification.

mRNA analysis by radioactive RT-PCR

FN cDNAs were generated using the cDNA synthesis kit (Amersham Biosciences) and alternative splicing of FN mRNA was quantitated via RT-PCR using primers in the exons flanking the EDA exon (FN2 Dir, 5′-ACCATCAC-CCTGTATGCTGTCT-3′ and EDA Rev, 5′-CTATGAGTCCTGACACAATCAC-3′) using a ^{32}P-dCTP in the PCR mix. RT-PCR products were analyzed by loading on 5% polyacrylamide gels, and the quantitative analysis of the PCR products were performed using a Cyclone PhosphorImager (Storage Phosphor System; Canberra Packard SRL). The values were corrected for background and G/C contents.

TUNEL analysis of skin wounds

Skin wounds at day 7 after wounding were analyzed with the TUNEL assay kit as described by the manufacturers (in situ Cell Death Detection Kit; Roche). In brief, skin sections were treated with terminal deoxynucleotidyl transferase and incubated with a solution containing the labeled nucleotide that was incorporated into cells having DNA breaks. The images were observed using a confocal microscope (Carl Zeiss MicroImaging, Inc.) and photographed under the same conditions of exposure and magnification (400×).

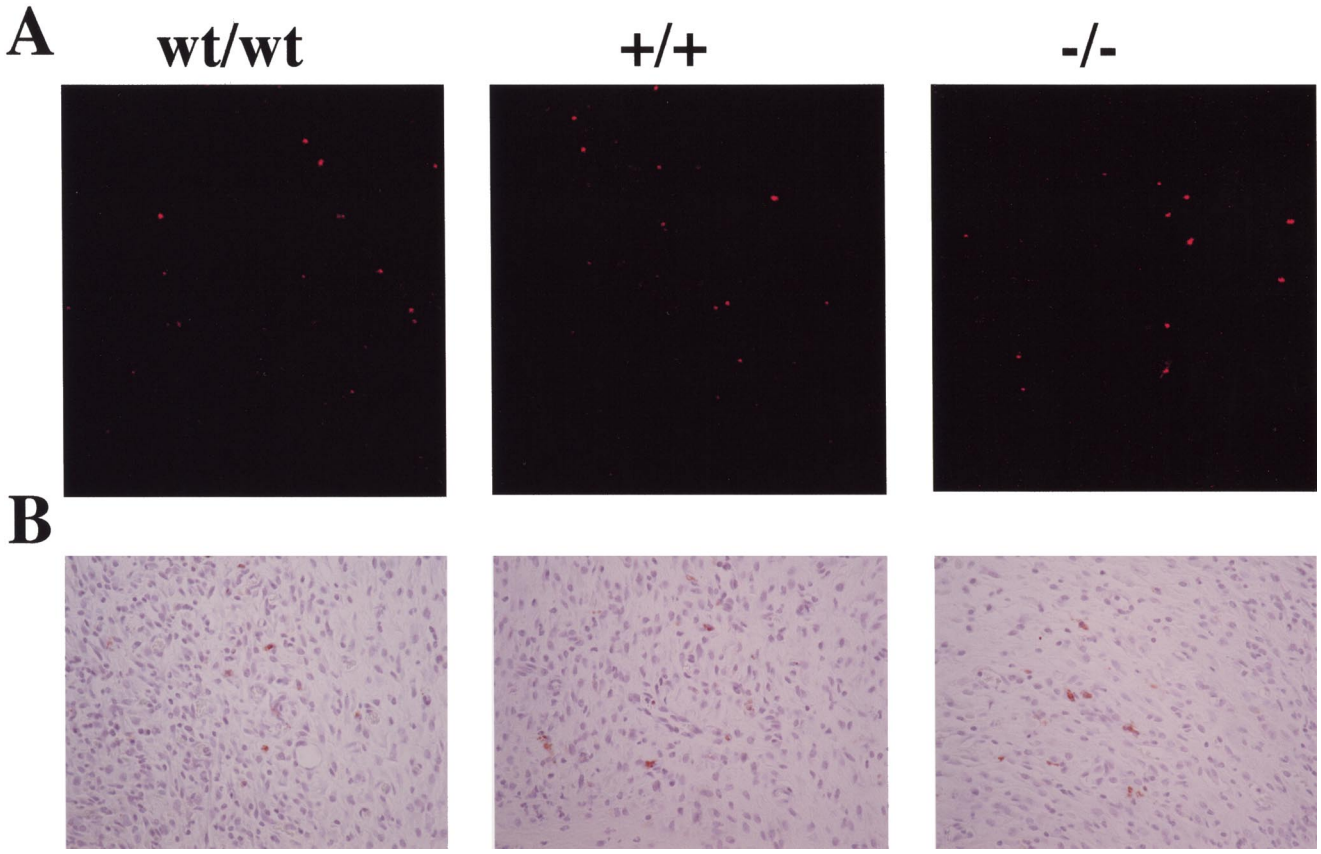

Figure S4. **TUNEL and caspase-3 analysis of wounded skin sections showed no differences in cell death between control ($EDA^{wt/wt}$) and mutant mice ($EDA^{+/+}$ and $EDA^{-/-}$).** (A) TUNEL analysis of full thickness cutaneous wounds. Full thickness cutaneous wounds of control ($EDA^{wt/wt}$, $n = 5$) and mutant mice ($EDA^{+/+}$ and $EDA^{-/-}$, $n = 4$ and 5, respectively) mice were analyzed at 7 d after wounding by the TUNEL assay as described by the manufacturers. The ulcerated areas presented a high number of positive cells (not depicted). No differences were observed between the genotypes in the nonulcerated areas. Representative sections of the granulation tissue area are shown. The experiment was repeated twice with similar results. (B) Caspase-3 immunohistochemistry showed no differences between the control mice ($EDA^{wt/wt}$) and mutant mice ($EDA^{+/+}$ and $EDA^{-/-}$). The same sections analyzed in A were stained with the anti–caspase-3 antibody. Photos show representative sections of the granulation tissue area.

Caspase-3 analysis of skin wounds

Serial sections of the same wounds used for the TUNEL assay were treated with the anti–caspase-3 antibody (Asp175; Cell Signaling). The samples were incubated with a peroxidase-conjugated secondary antibody by using the EnVision+ kit (DakoCytomation), and stained with the liquid DAB + substrate-chromagen solution (DakoCytomation) as suggested by the manufacturers. The images were observed and photographed at the same magnification (100×).

References

Ausubel, F.M., R. Brent, R.E. Kingston, D.D. Moore, G.J. Seidmann, J.A. Smith, and K. Struhl. 1998. Current protocols in molecular biology. John wiley and sons.

ffrench-Constant, C. 1995. Alternative splicing of fibronectin—many different proteins but few different functions. *Exp. Cell Res.* 221:261–271.

Hynes, R.O. 1990. Fibronectins. Springer-Verlag New York Inc., New York. 544 pp.

Kornblihtt, A.R., K. Vibe-Pedersen, and F.E. Baralle. 1984. Human fibronectin: molecular cloning evidence for two mRNA species differing by an internal segment coding for a structural domain. *EMBO J.* 3:221–226.

Kornblihtt, A.R., C.G. Pesce, C.R. Alonso, P. Cramer, A. Srebrow, S. Werbajh, and A.F. Muro. 1996. The fibronectin gene as a model for splicing and transcription studies. *FASEB J.* 10:248–257.

Laird, P.W., A. Zijderveld, K. Linders, M.A. Rudnicki, R. Jaenisch, and A. Berns. 1991. Simplified mammalian DNA isolation procedure. *Nucleic Acids Res.* 19:4293.

Muro, A.F., A. Iaconcig, and F.E. Baralle. 1998. Regulation of the fibronectin EDA exon alternative splicing. Cooperative role of the exonic enhancer element and the 5′ splicing site. *FEBS Lett.* 437:137–141.

Sambrook, J., E.F. Fritsch, and T. Maniatis. 1989. Molecular Cloning: A Laboratory Manual. Cold Spring Harbor Laboratory Press, Cold Spring Harbor, NY. 7.71–7.78.

Tamkun, J.W., and R.O. Hynes. 1983. Plasma fibronectin is synthesized and secreted by hepatocytes. *J. Biol. Chem.* 258:4641–4647.